Solar Energy 282 (2024) 112894

Contents lists available at ScienceDirect

Solar Energy

journal homepage: www.elsevier.com/locate/solener

# Flux density distribution forecasting in concentrated solar tower plants: A data-driven approach

Mathias Kuhl [a,b,*], Max Pargmann [a], Mehdi Cherti [b], Jenia Jitsev [b], Daniel Maldonado Quinto [a], Robert Pitz-Paal [a,c]

[a] *DLR, Institute of Solar Research, Linder Höhe, Köln, 51147, Germany*
[b] *FZJ, Jülich Supercomputing Centre, Wilhelm-Johnen-Straße, Jülich, 52428, Germany*
[c] *RWTH Aachen University, Chair of Solar Technology, Linder Höhe, Köln, 51147, Germany*

ARTICLE INFO

*Keywords:*
Solar power tower
Flux density prediction
Camera-target method
Heliostat
Machine learning

ABSTRACT

Concentrated Solar Power (CSP) systems, particularly those employing heliostat fields combined with a central tower, demonstrate substantial capacity for producing dispatchable, sustainable energy and fuel. This is achieved by focusing the sunlight with up to thousands of individual heliostats onto a single receiver. Forecasting the focal spot of each heliostat at any solar position becomes imperative to ensure optimal control. Nevertheless, the existing cutting-edge techniques aimed at predicting this flux density distribution either suffer from inaccuracies or entail substantial costs. In response to these challenges, our study introduces a novel approach involving a generative model that learns the shape and intensity patterns of the focal spots directly from images captured of the calibration target. We developed a purely data-driven methodology to generate the focal spots of the heliostats corresponding to various sun positions. The model is based on the StyleGAN architecture with adapted learnable input vectors for each individual heliostat and sun positions as input condition. The methodology's effectiveness is demonstrated through training and evaluation on data collected from a research power plant, where it achieved a flux prediction accuracy of 89% on the calibration target surface. Our work offers a novel solution for predicting flux density distributions in solar power plants in a fully data-driven way with a neural network. This method achieves cost efficiency by utilizing data obtained during standard operational procedures. Impressively, this method attains accuracy levels comparable to or exceeding those of current state-of-the-art techniques.

## 1. Introduction

Concentrated Solar Power (CSP), particularly solar power tower plants, represents a key technology in sustainable energy production, enabling dispatchable power generation and solar fuel production [1, 2]. These systems deploy thousands of heliostats, tracking the sun, to focus sunlight onto a central receiver, converting solar energy into thermal energy for a variety of use cases.

Critical to the operational efficiency and safety of CSP plants is the flux density distribution on the receiver. This distribution, a measure of the spatially distributed energy flux across the receiver's surface, affects the operational parameters and longevity of the receiver directly. Adhering to specific thermal thresholds and ensuring uniform energy absorption are essential to prevent damage and optimize the receiver's performance. Given that each receiver within CSP power plants has unique flux density distribution requirements, achieving an optimal balance between safety, durability, and thermal efficiency under variable solar conditions presents a significant challenge.

This challenge necessitates precise control over the flux density distribution, which relies on an in-depth knowledge of the characteristics of incoming solar radiation. The overall flux density distribution is a superposition of individual heliostat flux distributions, which can be adjusted and optimized through aiming of the heliostats [3–5]. However, the effectiveness of any aimpoint distribution algorithm hinges on accurate estimations of the focal spot shapes emitted by each heliostat. Traditional methods for predicting these focal spot characteristics, as summarized by Garcia et al. [6], such as Convolution Methods and Monte Carlo Raytracing, are limited by their accuracy and the costs involved. Consequently, more recent efforts have focused on leveraging direct measurements of the focal spots, captured in target images, to predict their intensity shapes with higher precision [7–12]. Despite advancements, issues with accuracy and scalability persist.

Addressing these challenges, our study introduces a novel, data-driven approach that employs a generative neural network to precisely

* Corresponding author at: DLR, Institute of Solar Research, Linder Höhe, Köln, 51147, Germany.
*E-mail address:* mathias.kuhl@dlr.de (M. Kuhl).

https://doi.org/10.1016/j.solener.2024.112894
Received 5 April 2024; Received in revised form 13 June 2024; Accepted 26 August 2024
Available online 5 September 2024

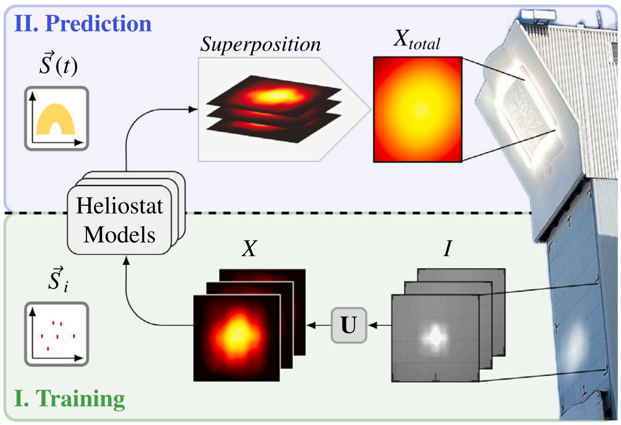


**Fig. 1.** Overview of data-driven methods for flux prediction using target images. Observed target images $I$, captured during the calibration process, are processed into flux distributions $X$. These flux measurements $X$, taken under various sun positions $\vec{S}_i$, facilitate the training of individual heliostat models. These models are then adept at forecasting changes in the shape of the focal spot for any sun position $\vec{S}(t)$, enabling the prediction of focal spots for each heliostat at any given time and their aggregation into the overall flux density $X_{total}$ on the receiver.

predict the irradiance profiles of heliostat focal spots under changing sun positions. Our approach employs a generalization strategy that utilizes comprehensive datasets from the entire heliostat field for thorough training of the neural network model. It distinguishes heliostat-specific characteristics through individual learnable parameters, derived from a minimal set of calibration images. These images include all necessary properties for accurately forecasting the heliostat's focal spot under any possible sun position. Notably, the heliostat properties are abstractly defined without necessitating a direct physical description; they are inferred in conjunction with the generative model during the training process. Utilizing images obtained during standard operational procedures enhances our method's cost-effectiveness and ease of deployment, seamlessly integrating with the conventional camera-target calibration process to improve flux prediction precision. By utilizing comprehensive datasets that cover the entire heliostat field, our approach not only boosts computational efficiency but also guarantees the model's scalability, allowing it to accommodate large heliostat arrays without a decline in performance.

In our work, we aim to progress towards the overall goal illustrated in Fig. 1 by analyzing whether purely data-driven models, devoid of physical modeling, can effectively predict flux and address the issues observed in earlier methods. Instead of predicting focal spots on the receiver and analyzing the total flux density, we evaluate the predictions on the calibration target itself. This approach allows us to leverage more accurate measurements and thoroughly assess this entirely new method, focusing specifically on single heliostat spot predictions.

## 2. State of the art

### 2.1. Camera-target calibration process

Our approach utilizes images acquired through the camera-target method, first introduced by Stone [13]. This process involves shifting the focal spot of a heliostat onto a Lambertian target located beneath the receiver. A strategically placed camera within the heliostat field captures the light reflected off the target, using the captured image to identify the focal spot's centroid. This information is crucial for adjusting a heliostat alignment model, enabling it to predict the focal spot's location based on the heliostat's actuator motor positions and the sun position. Recognized as a fundamental procedure in power plant operations for calibrating heliostats alignment models [14], its effectiveness has been validated in various studies, including work by Smith and Ho [15], Guangyu and Zhongkun [16] or Pargmann et al. [17].

### 2.2. Predicting heliostat focal spots

The calibration process yields models that predict the focal spot's center but are not capable of delineating its shape, crucial for adjusting the aimpoint distribution to account for mirror and facet canting deviations. Traditional methods for predicting focal spot shapes, as summarized by Garcia et al. [6], are Convolution Methods and Monte Carlo Raytracing.

Convolution methods, exemplified by Schwarzbözl et al. [18], apply mathematical superposition and convolution of error cones from individual heliostats. However, these idealized models are hampered by oversimplifications and assumptions, rendering them imprecise and unable to reflect the heliostat field's current state accurately. Monte Carlo Raytracing techniques, as employed by Leary and Hankins [19], Wendelin [20], Roccia et al. [21] or Belhomme et al. [22], also fall short when applied without consideration of heliostat surface deformations, failing to account for individual heliostat errors.

While raytracing simulations can be significantly improved through additional surface measurement techniques like deflectometric measurements [23] or photogrammetry [24,25], these methods face challenges with robustness to ambient conditions and are time-consuming, making them costly and impractical for large heliostat fields.

Recent methodologies exploit target images from a white Lambertian target to refine heliostat models. These images, rich in information about individual heliostat flux distributions, are ideal for developing heliostat flux prediction models without necessitating extra measurements, as they are routinely collected during daily operations within the calibration process.

One of the initial strategies to adjust heliostat models based on measured target images was introduced by Collado [7], utilizing a convolutional base model with heliostat focal spots represented as Gaussian distributions. This method adjusts the distribution's standard deviation according to observed focal spots for each heliostat to account for mirror and canting imperfections. Sánchez-González et al. [9] and Zhu et al. [10] proposed a more complex model that considers individual canted and focused mirror facets, fitting the model to focal spot measurements. While these techniques enable the monitoring of heliostat mirror errors over time, they rely on relatively simplistic heliostat models that cannot fully capture complex distortions within focal spots.

Rodríguez-Sánchez et al. [8] suggested a superposition method that employs measured focal spots directly, allowing for the capture of complex distortions within the flux distribution. However, this method's reliance solely on measured focal spots, without the ability to adjust for changing ambient conditions like sun position, necessitates hourly measurements for each heliostat, a requirement that renders it impractical for standard power plant operations, especially with large numbers of heliostats.

Addressing these challenges, Pargmann et al. [12] introduced a method that reconstructs a heliostat's surface deformations using a limited number of focal spot measurements (ranging from 2 to 16 target images). These deformations are represented as $4 \times 7 \times 7$ parameters formulated in differentiable splines. This approach facilitates accurate raytracing simulations of heliostat behavior under various conditions, leading to precise focal spot predictions. Nonetheless, it demands optimizing the heliostat surface through differentiable raytracing for each heliostat individually, increasing computation time significantly, making it impractical for entire heliostat fields. Moreover, the canting and focusing of heliostat mirrors result in greater flux distribution overlap, complicating surface reconstruction from focal spots for heliostats distant from the calibration target.

In addressing the challenges of reconstructing images over greater distances between the heliostat and the target surface, where the focal point is observed, Martínez-Hernández et al. [11] adopted a methodology similar to that of Pargmann et al. [12]. Their innovative approach involved the deployment of a movable target, strategically placed directly in front of the heliostat, enabling the precise calculation of its surface deformations. Nevertheless, this method necessitated the use of a vehicle to navigate through the heliostat field, thereby elevating the operational costs and limiting its feasibility for implementation across extensive heliostat fields.

Therefore, we propose a generalizing data-driven approach to address several shortcomings of previous methods. Data-driven, in this context, means that we directly use focal spot measurements to predict changes under different conditions, bypassing the need for physically motivated heliostat modeling. Pargmann et al. [12] have demonstrated in their research that it is possible to predict focal spots from surfaces that are optimized to those focal spots, even if the derived surfaces are not correct. Consequently, we aim to identify the parameters that describe heliostat properties in an abstract, more efficient, and suitable manner. By directly training models on measured focal spots, we can capture all details in the flux distribution prediction without relying on simplified models. We adopt a generalizing approach, training a single model for the entire heliostat field, which renders our method both efficient and easily scalable to large heliostat fields.

## 3. Method

Reflecting the primary goal outlined in Fig. 1, we employ target images obtained through the camera-target calibration process. These images are converted into flux density distributions using a UNet model, as detailed in Kuhl et al. [26]. By utilizing focal spot measurements from various sun positions, we derive models for individual heliostats, enabling the prediction of focal spot changes for any given sun position. This facilitates the forecasting of each heliostat's focal spots at any moment. Unlike the methodology in Fig. 1, we focus on predictions on the calibration target itself rather than the receiver. This enables a more accurate and controlled analysis of this new purely data-driven methodology.

### 3.1. Data-driven approach

Our method is entirely data-driven, devoid of any physical descriptions of heliostats, such as mirror surface attributes. Instead, the model learns the variability of focal spots based on calibration image data and changing input conditions. Mathematically, this is expressed as:

$$X = \mathbf{G}(\tilde{H}_i, \vec{S}) \tag{1}$$

where $X$ represents the focal spot, dependent on heliostat parameters $\tilde{H}_i$ and sun position $\vec{S}$. These heliostat parameters $\tilde{H}_i$ abstractly encode the unique properties necessary for computing the focal spot for each heliostat $H_i$. Our model, $\mathbf{G}$, is trained to generate the focal spot $X$ based on these inputs. It is crucial to note that the focal spot's intensity distribution shape is influenced not only by the sun's position but also by changes in the aim point. Our study circumvents this by focusing on measurements with nearly consistent aim points, by using only data for training and prediction from the same calibration target. Moreover, our model is designed to be independent of conditions such as the Direct Normal Irradiance (DNI) and mirror reflectivity, which are traditionally factors in flux scaling. To achieve this, we normalize all focal spots $X$ to a mean pixel value of 0.5 for model training. This standardization ensures each focal spot represents a uniform normalized energy flux, allowing the model to focus solely on predicting the shape of the focal spots without the influence of external scaling factors. For the superposition of individual focal spots into the total flux distribution $X_{total}$, a heliostat energy model, as outlined in Kuhl et al. [26], can be used to convert relative intensity values into absolute flux predictions in $\mathrm{W\,m^{-2}}$ for each focal spot. Since our work focuses on predicting the flux distributions of single heliostat focal spots, this step is not necessary in our study.

### 3.2. Dataset

The base of any machine learning approach, particularly those that are data-driven, is the underlying dataset. Consistent with Eq. (1), our aim is to predict the focal spots $X$ of different heliostats $H_i$ across various sun positions $\vec{S}$, requiring a dataset that covers this spectrum of conditions.

Our dataset is sourced directly from the calibration process conducted during power plant operation of the research power plant Solar Tower Jülich [27]. This process yields approximately 120,000 target images over the span of one year, covering around 1000 heliostats. Our dataset was collected throughout the year 2022. Each captured image is cataloged with the corresponding heliostat ID $H_i$ and the corresponding sun position $\vec{S}$. These images are then processed to derive relative flux distributions $X$ utilizing the UNet framework as described in Kuhl et al. [26]. To streamline our analysis, we select only those heliostats with a minimum of 35 target images. This selection is further distilled into 25 images for model training purposes and 10 for testing for each heliostat. We selected a maximum of 25 training images, as our observations indicated that increasing the number beyond this did not enhance the training outcomes. Additionally, we utilized only 10 test images, as we deemed this quantity sufficient to provide a comprehensive range for evaluation. Such segmentation into training and testing groups is essential within machine learning to foster model learning from a dedicated dataset and to gauge its generalization across unseen data, effectively reducing the likelihood of model overfitting.

In instances where heliostats are documented with over 35 measurements, we refine the dataset to include only the 35 data points that exhibit the greatest variance in sun positions, employing an algorithm designed to maximize the spatial separation in terms of azimuth and elevation. This approach guarantees that our testing subset includes 10 data points for each heliostat, spanning a broad array of sun positions. This breadth ensures our model's predictions are evaluated over a comprehensive spectrum of conditions likely to be encountered in operational environments.

Post-filtering, the dataset is consolidated to include 605 heliostats, each represented by 25 training images and 10 testing images, cumulating to a total of 21,175 target images for the study.

Even though our method is independent of physical modeling and parameters, we present a short description of the heliostats used at the STJ power plant. These heliostats consist of four rectangular facets, each with an area of 1.92 $\mathrm{m}^2$. The facets are canted towards the receiver and are non-focusing.

### 3.3. Model implementation

In line with the principles outlined in Eq. (1), we aim to synthesize images $X$ based on the input conditions $\tilde{H}_i$ and $\vec{S}$, formulated as multidimensional vectors. The StyleGAN architecture, as referenced in the work of Karras et al. [28], emerges as an ideal solution for this task. It utilizes input vectors to direct the generation process across various scales, managing both large scale features and small scale details independently. This capability is particularly advantageous for creating and forecasting focal spots, enabling the model to capture their nuances at different resolutions.

We have tailored the StyleGAN architecture to address our unique challenge, as depicted in Fig. 2. Recognizing that each heliostat's mapping to its focal spot under specific sun positions is distinct, we eliminate the inherent randomness typically employed within the StyleGAN model to produce a variety of images. This involves removing both the random input vector and any additional noise layers, substituting them with targeted heliostat parameters and sun positions, both represented as vectors. Additionally, this unique mapping between inputs and outputs led us to eliminate the discriminator component, which we found did not enhance the results in our research.

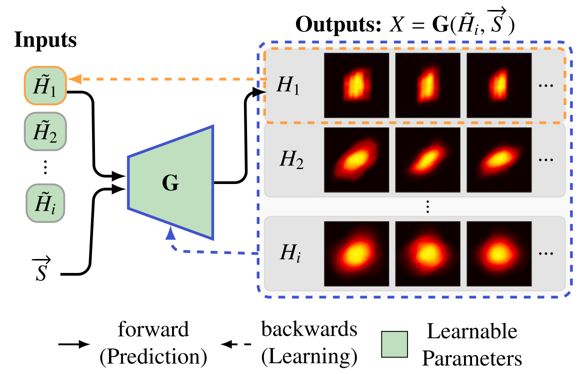


**Fig. 2.** Adapted StyleGAN architecture for focal spot prediction. This diagram illustrates how heliostat properties, represented as vectors $\tilde{H}_i$, and sun position vectors $\vec{S}$, feed into the StyleGAN generator **G** to produce focal spots. The process involves comparing predicted focal spots with actual measurements to inform the training loss. Each heliostat's specific parameters $\tilde{H}_i$ are fine-tuned based on its associated focal spots, whereas the generator **G** is universally trained across the entire dataset.

Given the extensive amount of images required for usual applications of StyleGAN training, which often exceeds thousands of images, our dataset for any single heliostat proves insufficient in diversity and volume. To circumvent this, we adopt a generalizing training approach for our generator **G**, incorporating learnable heliostat parameters $\tilde{H}_i$ as supplementary inputs. This method allows each heliostat's vector $\tilde{H}_i$ to be individually calibrated during training, while the generator **G** benefits from the aggregate data across all heliostats. Consequently, the generator acquires a generalized understanding of focal spot variations under different solar conditions, embedding specific heliostat characteristics within the vectors $\tilde{H}_i$. These vectors abstractly encode all pertinent heliostat attributes, without resorting to a concrete physical representation, yet still containing unique essential information for accurate focal spot forecasting under varying sun positions.

Training involves processing images from our dataset, each tagged with a heliostat ID $H_i$, a solar position $\vec{S}$, and the corresponding focal spot $X$. The ID $H_i$ selects the corresponding heliostat properties vector $\tilde{H}_i$, which is then combined with $\vec{S}$ to inform the generator's input. The generator **G** then predicts the focal spot $X$ for the heliostat under the specific sun position. Predictions are evaluated against actual measured focal spots $\hat{X}$ using a pixel-wise L2-Loss, facilitating both generator **G** training and specific heliostat parameter $\tilde{H}_i$ adjustments. Thus, while updates to the generator **G** are influenced by the entire dataset, updates to a heliostat's parameters $\tilde{H}_i$ are dictated solely by its own images.

This generalizing strategy not only economizes data usage for the generative model but also fosters synergy and knowledge exchange among heliostats, enriching individual heliostat models. Given the vast number of heliostats, each with similar defects and deformations, this approach facilitates the sharing of observed errors and attributes, promoting a cohesive heliostat field model. By using an abstract model for heliostats, we avoid the complex details of surface deformations. This approach has been supported by Pargmann et al. [12], described in 2.2, who showed that even with surfaces derived inaccurately, it is still possible to make precise predictions about focal spots. Therefore, choosing this simplified methodology allows us to more efficiently predict changes in the shape and structure of focal spots.

## 4. Results

In our analysis, we directly assess the model's performance on the test dataset to determine its accuracy in predicting unseen focal spots, which were not part of the network's training. Fig. 3 presents a comparison of predicted flux distributions $X$ against the actual measurements $\hat{X}$ for five distinct heliostats $H_i$, each at varying distances from the target $d$. It can be noted that the focal spots are accurately predicted across all distances. However, for heliostats positioned very closely, while the overall shape and distribution of the predicted focal spot are precise, some fine details may be absent. Below each image, the pixel-wise loss $L$ quantifies the discrepancy between the model's predictions and the ground truth, which is defined as the mean devitation between predicted and groundtruth flux and scaled by the mean intensity:

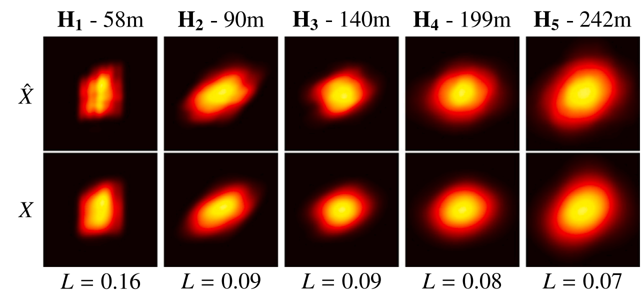


**Fig. 3.** Normalized flux prediction versus measured ground truth. This figure displays flux predictions $X$ alongside the actual measurements $\hat{X}$ for five distinct heliostats $H_i$, each located at varying distances $d$ from the target. For each heliostat, one example is presented, illustrating the model's prediction accuracy. The calculated loss $L$ quantifying the difference between the prediction and the ground truth is provided beneath each image comparison.

$$L = \frac{\sum_i |X_i - \hat{X}_i|}{\sum_i \hat{X}_i} \tag{2}$$

Here, $X$ represents the predicted focal spot and $\hat{X}$ its groundtruth value, $i$ represents pixel indices. We chose this measure because, compared to methods using contour lines for comparison, the pixel-wise flux error allows us to directly and quantitatively evaluate errors in the spatially resolved flux. This loss function is independent of image resolution, as changes in resolution proportionally affect both the numerator and denominator. Additionally, areas with flux close to zero have minimal impact on the loss because we sum all deviations first and then normalize. This normalization ensures that all focal spots have the same total energy, regardless of their distribution. Consequently, whether the focal spots are from near or distant heliostats does not influence the loss, because it is independent of the ratio between the focal spot size and the image size.

### 4.1. Accuracy evaluation

The test set reveals how our model manages to accurately capture the shape of focal spots for a wide range of heliostats positioned at varying distances from the tower. Closer heliostats display more intricate details due to mirror surface deformations, whereas these details diminish for heliostats situated further away, attributed to the sun's irradiation opening angle and the overlapping effects from different heliostat facets due to canting or focusing. Across our dataset of 605 heliostats, this evaluation method yields an average relative flux error $\overline{L}$ of approximately 9.7%, translating to a relative flux prediction accuracy of 90%.

### 4.2. Distance impact analysis

By categorizing heliostats based on their distance to the target, ranging from 50 to 250 m in 50 m increments, we observed that prediction accuracy improves with increased distance. This trend, illustrated in Fig. 4, suggests that focal spots of heliostats further from the tower are less complex and thus easier to predict, with the prediction error for heliostats located 50–100 m away at 10%, and for those 200–250 m away at 9%, indicating a modest 1% change in accuracy depending on the distance.

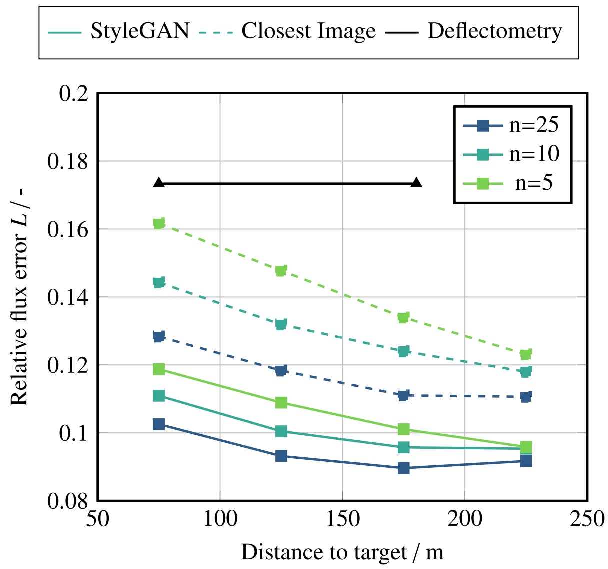


**Fig. 4.** Comparison of flux prediction error across methods for heliostats at varying distances from the tower. This figure illustrates the performance of our StyleGAN approach versus the Closest Image method across three scenarios based on the number of available images per heliostat ($n = 5, 10, 25$). Additionally, the Deflectometry combined with Raytracing method is evaluated for two distance groups, limited by the availability of deflectometry data.

### 4.3. Training data volume impact

Further experiments explored the effect of reducing the number of training images per heliostat from 25 to 10 and then to 5. We observed a uniform increase in prediction error by approximately 0.5% with each reduction. Our model's accuracy peaks with around 25 images per heliostat and does not benefit from additional data.

### 4.4. Comparison with other methods

Our approach was also compared against a Closest Image method, which predicts focal spots based on the nearest image in terms of sun position. In our case we predict the test samples from the closest measurement in our training set. This method, akin to the Superposition method by Rodríguez-Sánchez et al. [8], exhibited prediction errors ranging from 11%–13% across different groups, underscoring the superior accuracy of our StyleGAN model compared to the Closest Image method. Even a StyleGAN model trained with only 5 images per heliostat outperforms the Closest Image method with 25 image samples per heliostat.

We also evaluated our model against a method incorporating deflectometry measurements and raytracing, deemed the most accurate in literature [22], though limited by their time-intensive and error-prone nature. Our study, limited to 83 heliostats owing to measurement difficulties, focused on distances ranging from 50 to 180 meters to the target. Given the absence of a discernible trend in $L$ relative to distance in our deflectometry-based predictions, we reported a consistent mean value of 17.3% across all distances. Although we used the same method as Belhomme et al. [22], we were unable to achieve high accuracies for all heliostats across all measurements due to the method's robustness. Fig. A.6 shows several samples of focal spot predictions using deflectometry-based ray tracing. While the simulations accurately predict the general characteristics of the focal spot shapes, they lack precise spatial resolution.

The results reveal that our StyleGAN approach outperforms deflectometry-based predictions by approximately 7.6%, even with as few as 5 images per heliostat. With the remark that in this study we evaluated both methods not on the receiver but on the calibration target, where methods utilizing exactly those images have advantages.

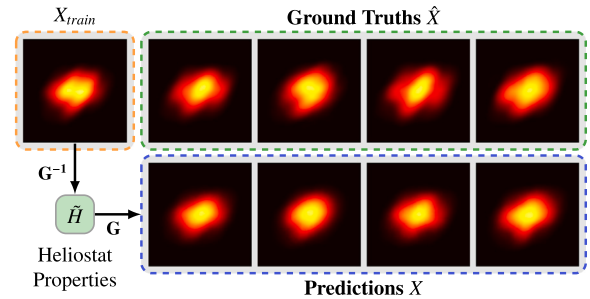


**Fig. 5.** Single image prediction test. This figure demonstrates the model's ability to derive heliostat properties $\tilde{H}$ from a single training image $X_{train}$. The derived $\tilde{H}$ is subsequently utilized to predict focal spots for varying sun positions for a specific heliostat. Predicted focal spots are then compared to their actual measured ground truth $\hat{X}$.

### 4.5. Enhanced generalizing capabilities

In a targeted experiment to assess our model's generalizing abilities and to test if the generalizing approach enables synergys between heliostat datasets, we explored its capacity to deduce heliostat characteristics from a single image and predict changes in focal spots due to varying sun positions. This test was pivotal in evaluating the model's adaptability to new scenarios based on limited initial data.

The findings show the model's capability to accurately anticipate focal spot modifications across different solar alignments from just one training image, as shown in Fig. 5. Such an outcome not only attests to the model's skill in acquiring a broad understanding of focal spot behavior but also its proficiency in applying learned insights across different heliostats. This ability to transfer knowledge enhances the model's efficiency, particularly in large-scale settings where exhaustive data collection for each heliostat is not feasible.

Moreover, the model's success with minimal data inputs suggests significant practical benefits, especially in operational contexts where data acquisition is challenging. It implies a reduction in both the resources and the time required for model training and recalibration.

## 5. Discussion

Our investigation into flux density forecasting within concentrated solar tower plants introduces a novel data-driven methodology, leveraging a generative model to understand and predict the complex variability in focal spots caused by changing sun positions. This approach addresses the limitations of traditional prediction methods by incorporating the versatility and depth of machine learning, specifically through the adaptation of the StyleGAN architecture, to derive a model capable of generalizing focal spot prediction.

The capacity to predict these focal spots with high precision – evidenced by an 90% accuracy – marks a significant advancement over previous methods. Notably, our method's ability to generalize from limited data points and to accurately infer heliostat behavior from a minimal dataset underscores its potential for practical application. We outperform earlier methods in accuracy and still guarantee easy application and good scalability by training one generalizing model for the whole heliostat field.

It is important to note that this method is trained and evaluated on the target plane. Therefore, for precise prediction on the receiver, we have to account for an additional error due to aimpoint change. We have simulated this error in a raytracing environment and found that this aimpoint change of 10 m results in an additional error of 2% for far heliostats and 10% for close heliostats.

## 6. Conclusion and outlook

This study presents a novel, data-driven approach to flux density forecasting in concentrated solar tower plants, achieving significant improvements in prediction accuracy and operational efficiency. By harnessing the power of a generative neural network, we have developed a model that learns from the intrinsic patterns of heliostat focal spots, enabling accurate forecasting across varying sun positions from limited data.

Our findings not only demonstrate the model's effectiveness in surpassing traditional prediction methods but also highlight its generalizing capabilities, offering a scalable solution that is easily applicable to many heliostats. Training the generative model with data from the entire heliostat field facilitates synergies among individual heliostat models and diminishes the total amount of required data. We have shown that we can predict the characteristics of focal spots without the need for deriving physical heliostat properties, like surface deformations.

Our method can seamlessly be integrated into the standard heliostat calibration process using the camera-target method. Therefore, we can extend heliostat models acquired from the calibration process by not only predicting the alignment but also providing an accurate prediction of the focal spots' shape. This method not only enhances the overall accuracy of flux predictions but also enables more efficient receiver operation and longer-lasting components through improved aimpoint control.

This method is just a first step towards data-driven flux prediction. We have showcased the method by training and evaluation on the target plane. Ongoing work should focus on including aimpoints in the model to be able to get more accurate extrapolations of flux predictions on the receiver derived from calibration target data. Also, future work should investigate how we can account for complex receiver surfaces or even cavity reactors within a data-driven flux prediction method.

## CRediT authorship contribution statement

**Mathias Kuhl:** Writing – review & editing, Writing – original draft, Visualization, Validation, Software, Methodology, Investigation, Formal analysis, Data curation, Conceptualization. **Max Pargmann:** Writing – review & editing, Supervision, Conceptualization. **Mehdi Cherti:** Methodology. **Jenia Jitsev:** Writing – review & editing, Methodology. **Daniel Maldonado Quinto:** Writing – review & editing, Supervision, Project administration, Methodology, Conceptualization. **Robert Pitz-Paal:** Supervision, Funding acquisition.

## Declaration of competing interest

The authors declare that they have no known competing financial interests or personal relationships that could have appeared to influence the work reported in this paper.

## Acknowledgments

We gratefully acknowledge the use of data from the Solar Tower in Jülich, a research power plant operated by the German Aerospace Center (DLR). Additionally, we extend our thanks for the funding provided by the Helmholtz Association (HGF), Germany for the *GANCSTR* project (Grant Number ZT-I-PF-5-069), under which this research was conducted.

## Appendix. Examples of focal spot predictions based on deflectometry measurements

See Fig. A.6.

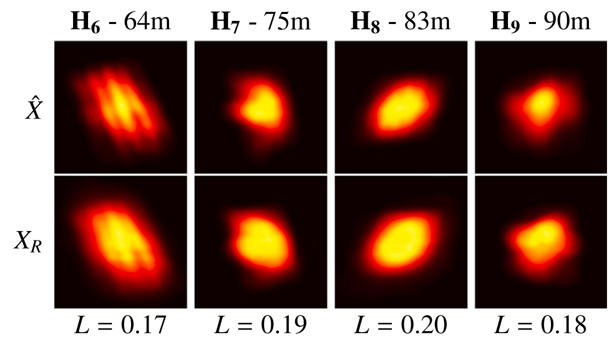


**Fig. A.6.** Normalized flux prediction versus measured ground truth. This figure displays flux predictions $X_R$, simulated from deflectometry enhanced raytracing, alongside the actual measurements $\hat{X}$ for four distinct heliostats $H_i$. For each heliostat, one example is presented, illustrating the model's prediction accuracy. The calculated loss $L$ quantifying the difference between the prediction and the ground truth is provided beneath each image comparison.

## References


[1] F. Schöniger, R. Thonig, G. Resch, J. Lilliestam, Making the sun shine at night: comparing the cost of dispatchable concentrating solar power and photovoltaics with storage, Energy Sources,Part B: Econ. Plann. Policy 16 (1) (2021) 55–74.

[2] R. Schäppi, D. Rutz, F. Dähler, A. Muroyama, P. Haueter, J. Lilliestam, A. Patt, P. Furler, A. Steinfeld, Drop-in fuels from sunlight and air, Nature 601 (7891) (2022) 63–68.

[3] A. Sánchez-González, M.R. Rodríguez-Sánchez, D. Santana, Aiming factor to flatten the flux distribution on cylindrical receivers, Energy 153 (2018) 113–125.

[4] L. Oberkirsch, D. Maldonado Quinto, P. Schwarzbözl, B. Hoffschmidt, GPU-based aim point optimization for solar tower power plants, Sol. Energy 220 (2021) 1089–1098.

[5] Y. Wang, Z. Wu, D. Ni, Real-time optimization of heliostat field aiming strategy via an improved swarm intelligence algorithm, Appl. Sci. 14 (1) (2024) 416.

[6] P. Garcia, A. Ferriere, J.-J. Bezian, Codes for solar flux calculation dedicated to central receiver system applications: A comparative review, Sol. Energy 82 (3) (2008) 189–197.

[7] F.J. Collado, One-point fitting of the flux density produced by a heliostat, Solar Energy 84 (4) (2010) 673–684.

[8] M.d.l.R. Rodríguez-Sánchez, C. Leray, A. Toutant, A. Ferriere, G. Olalde, Development of a new method to estimate the incident solar flux on central receivers from deteriorated heliostats, Renew. Energy 130 (2019) 182–190.

[9] A. Sánchez-González, B. Grange, C. Caliot, Computation of canting errors in heliostats by flux map fitting: experimental assessment, Opt. Express 28 (26) (2020) 39868–39889.

[10] R. Zhu, D. Ni, T. Yang, J. Yang, J. Chen, G. Xiao, Heliostat field aiming strategy optimization with post-installation calibration, Appl. Therm. Eng. 202 (2022) 117720.

[11] A. Martínez-Hernández, R. Conceição, C.-A. Asselineau, M. Romero, J. González-Aguilar, Advanced surface reconstruction method for solar reflective concentrators by flux mapping, Sol. Energy 266 (2023) 112162.

[12] M. Pargmann, J. Ebert, M. Götz, D. Maldonado Quinto, R. Pitz-Paal, S. Kesselheim, Automatic heliostat learning for in situ concentrating solar power plant metrology with differentiable ray tracing, Nature Commun. 15 (1) (2024) 6997.

[13] K.W. Stone, Automatic heliostat track alignment method, 1986, US Patent 4, 564, 275.

[14] J.C. Sattler, M. Röger, P. Schwarzbözl, R. Buck, A. Macke, C. Raeder, J. Göttsche, Review of heliostat calibration and tracking control methods, Sol. Energy 207 (2020) 110–132.

[15] E. Smith, C. Ho, Field demonstration of an automated heliostat tracking correction method, Energy Procedia 49 (2014) 2201–2210.

[16] L. Guangyu, C. Zhongkun, Heliostat attitude angle detection method based on BP neural network, in: MATEC Web of Conferences, Vol. 139, EDP Sciences, 2017, p. 00043.

[17] M. Pargmann, M. Leibauer, V. Nettelroth, D. Maldonado Quinto, R. Pitz-Paal, Enhancing heliostat calibration on low data by fusing robotic rigid body kinematics with neural networks, Sol. Energy 264 (2023) 111962.

[18] P. Schwarzbözl, R. Pitz-Paal, M. Schmitz, Visual HFLCAL-a software tool for layout and optimisation of heliostat fields, in: Proceedings, 2009.

[19] P. Leary, J. Hankins, User's guide for MIRVAL: a computer code for comparing designs of heliostat-receiver optics for central receiver solar power plants, Technical Report, Sandia National Lab.(SNL-CA), Livermore, CA (United States), 1979.

[20] T. Wendelin, Soltrace: a new optical modeling tool for concentrating solar optics, in: International Solar Energy Conference, Vol. 36762, 2003, pp. 253–260.

[21] J. Roccia, B. Piaud, C. Coustet, C. Caliot, E. Guillot, G. Flamant, J. Delatorre, SOLFAST, a ray-tracing Monte-Carlo software for solar concentrating facilities, in: J. Phys. Conf. Series, 369, IOP Publishing, 2012, 012029.

[22] B. Belhomme, R. Pitz-Paal, P. Schwarzbözl, S. Ulmer, A new fast ray tracing tool for high-precision simulation of heliostat fields, J. Solar Energy Eng. 131 (3) (2009) 031002.

[23] S. Ulmer, T. März, C. Prahl, W. Reinalter, B. Belhomme, Automated high resolution measurement of heliostat slope errors, Sol. Energy 85 (4) (2011) 681–687.

[24] M. Röger, C. Prahl, S. Ulmer, Fast determination of heliostat shape and orientation by edge detection and photogrammetry, in: Proc. 14th CSP SolarPACES Symposium 2008, SolarPACES, 2008.

[25] A. Bonanos, M. Faka, D. Abate, S. Hermon, M. Blanco, Heliostat surface shape characterization for accurate flux prediction, Renew. Energy 142 (2019) 30–40.

[26] M. Kuhl, M. Pargmann, M. Cherti, J. Jitsev, D. Maldonado Quinto, R. Pitz-Paal, In-situ UNet-based heliostat beam characterization method for precise flux calculation using the camera-target method, Sol. Energy 279 (2024) 112811.

[27] S. Pomp, P. Schwarzbözl, G. Koll, F. Göhring, T. Hartz, M. Schmitz, B. Hoffschmidt, The solar tower jülich – first operational experiences and test results, in: Proceedings of the SolarPACES 2010 Conference, Perpignan, France, 2010.

[28] T. Karras, S. Laine, T. Aila, A style-based generator architecture for generative adversarial networks, in: Proceedings of the IEEE/CVF Conference on Computer Vision and Pattern Recognition, 2019, pp. 4401–4410.